Multifunctional Biomimetic Nanovaccines Based on Photothermal and Weak-Immunostimulatory Nanoparticulate Cores for the Immunotherapy of Solid Tumors

Li, Jiachen

2022-03

Multifunctional Biomimetic Nanovaccines Based on Photothermal and Weak-Immunostimulatory Nanoparticulate Cores for the Immunotherapy of Solid Tumors

Jiachen Li, Di Huang, Ruoyu Cheng, Patrícia Figueiredo, Flavia Fontana, Alexandra Correia, Shiqi Wang, Zehua Liu, Marianna Kemell, Giulia Torrieri, Ermei M. Mäkilä, Jarno J. Salonen, Jouni Hirvonen, Yan Gao, Jialiang Li, Zhenyang Luo,* Hélder A. Santos,* and Bing Xia*

An alternative strategy of choosing photothermal and weak-immunostimulatory porous silicon@Au nanocomposites as particulate cores to prepare a biomimetic nanovaccine is reported to improve its biosafety and immunotherapeutic efficacy for solid tumors. A quantitative analysis method is used to calculate the loading amount of cancer cell membranes onto porous silicon@Au nanocomposites. Assisted with foreign-body responses, these exogenous nanoparticulate cores with weak immunostimulatory effect can still efficiently deliver cancer cell membranes into dendritic cells to activate them and the downstream antitumor immunity, resulting in no occurrence of solid tumors and the survival of all immunized mice during 55 day observation. In addition, this nanovaccine, as a photothermal therapeutic agent, synergized with additional immunotherapies can significantly inhibit the growth and metastasis of established solid tumors, via the initiation of the antitumor immune responses in the body and the reversion of their immunosuppressive microenvironments. Considering the versatile surface engineering of porous silicon nanoparticles, the strategy developed here is beneficial to construct multifunctional nanovaccines with better biosafety and more diagnosis or therapeutic modalities against the occurrence, recurrence, or metastasis of solid tumors in future clinical practice.

1. Introduction

Cancer immunotherapies like immune checkpoint blockade (ICB) therapies, cellular therapies based on engineered immune-related cells, and cancer vaccines can boost antitumor immune responses to inhibit cancer occurrence. Compared with other immunotherapeutic strategies, cancer vaccines including whole cell vaccine, peptide vaccine, genetic engineering vaccine, and antibody vaccine have relatively low economic cost and high specificity to attack tumor cells with low side effects, leading to their successes in the clinic.[1] With the introduction of tumor-relevant antigens and adjuvants, cancer vaccines can activate antigen-presenting cells (APCs) such as dendritic cells (DCs), and T cells including CD8+ cytotoxic T lymphocytes (CTLs) and CD4+ helper T lymphocytes (Th) to trigger antigen-specific antitumor immunity in the body with the secretion of

J. Li, D. Huang, Y. Gao, J. L. Li, Z. Luo, B. Xia
College of Science
Nanjing Forestry University
Nanjing 210037, China
E-mail: luozhenyang@njfu.edu.cn; xiabing@njfu.edu.cn
J. Li, R. Cheng, P. Figueiredo, F. Fontana, A. Correia, S. Wang, Z. Liu,
G. Torrieri, J. Hirvonen, H. A. Santos
Drug Research Program
Division of Pharmaceutical Chemistry and Technology
University of Helsinki
Helsinki FI-00014, Finland

J. Li, H. A. Santos
Department of Biomedical Engineering and W.J. Kolff Institute for
Biomedical Engineering and Materials Science
University of Groningen/University Medical Center Groningen
Ant. Deusinglaan 1, Groningen 9713 AV, The Netherlands
E-mail: h.a.santos@umcg.nl
M. Kemell
Department of Chemistry
University of Helsinki
Helsinki FI-00014, Finland
E. M. Mäkilä, J. J. Salonen
Laboratory of Industrial Physics
Department of Physics and Astronomy
University of Turku
Turku FI-20014, Finland

pro-inflammatory cytokines.[2,3] Recently, nanovaccines based on inorganic, organic, polymers, and bio-macromolecule nanoparticles (NPs) with their strong inherent immunostimulatory effects or loading additional adjuvant agents have been used to delivery tumor antigens and activate downstream immune responses.[4–9] In contrast to single-antigen nanovaccines and whole cancer cell vaccines, cancer cell membranes (CCM), as the source of mutiantigenic materials without the disturbance of others cell inclusions,[10] can be cloaked onto potent immunological nanoparticulate cores to stimulate multiantigenic immunities with enhanced tumor specificity, called "biomimetic nanovaccines."[11–13] Considering that CCM can eventually be derived from the patient's own tumors, these biomimetic nanovaccines have important potential on the personalized therapy of cancer.[14–16] However, once these nanovaccines go through lymphatic capillary into blood capillary, the leakage of their immunostimulatory adjuvants usually induces unacceptable systemic inflammation.[17–19] Therefore, to avoid this high risk, it is necessary to develop biomimetic nanovaccines based on weak- or non-immunostimulatory nanoparticulate cores.

Established solid tumors with weak immune responses are particularly challenging for immunotherapies because of their physical barriers of dense extracellular matrix and physiological barriers of immunosuppressive tumor microenvironments (TME).[20–22] Recently, photothermal therapy synergized with immunotherapy has been developed as a novel therapeutic modality against the growth and metastasis of established solid tumors.[23–26] This is because photothermal therapy can not only destroy their extracellular matrices and reverse their immunosuppressive TME to sensitize them for immunotherapies, but also induce the immunologic death of tumor cells to activate antitumor responses in the body. When primary solid tumors are seated in deep tissues, photothermal therapy can be also conveniently coordinated with interventional techniques including optical fibers and endoscopy to avoid the operation of laparotomy and thoracotomy.[27] Accordingly, photothermal therapeutic modality is suggested to be integrated with nanovaccines, aiming to treat the occurrence, recurrence, and metastasis of established solid tumors. In our previous studies,[28] biocompatible and biodegradable porous silicon NPs (PSiNPs) with oxidation or hydrocarbonization treatments show a significant immunostimulatory effect on immune cells, such as enhancing the activation of DCs, the proliferation of T cells, and the secretion of cytokines. On this basis, oxidized PSiNPs with a strong intrinsic immunostimulatory effect and loading additional immunostimulant agents were coated with CCM to construct PSiNP-based biomimetic nanovaccines.[29–31] Here, an alternative strategy of choosing photothermal and weak-immunostimulatory porous silicon@Au nanocomposites as particulate cores to obtain a CCM@(PSiNPs@Au) nanovaccine is developed, as shown in Scheme S1a,b (Supporting Information). Their stimulation on antitumor immune responses to inhibit the proliferation of tumor cells in vitro and the occurrence of solid tumors in vivo were studied. Finally, combined with ICB immunotherapy, CCM@(PSiNPs@Au) nanovaccine as a photothermal therapeutic agent against the growth and metastasis of established solid tumors was also studied in vivo.

2. Results and Discussion

First, PSiNPs were produced by electrochemically etching Si wafers, after which the obtained material was wet-milled in toluene using a high-energy ball mill to prepare hydrogen-terminated PSiNPs under nitrogen protection. Next, Au^{3+} ions of $HAuCl_4$ were in situ reduced by surface Si—H moieties of PSiNPs at 60 °C, to obtain PSiNPs@Au nanocomposites. This in situ reductive method has been reported to incorporate Au NPs onto silicon-based nanomaterials including silicon nanowires, porous silicon nanopillars, porous silicon nanodisks, or PSiNPs.[32–35] PSiNPs@Au nanocomposites prepared with different mass ratios between PSiNPs and $HAuCl_4$ precursor solution ($m_{Si}:m_{Au}$) were monitored by scanning electron microscopy (SEM) with an energy-dispersive spectroscopy (EDS). From Figure S1a,b (Supporting Information), with the changing of the mass ratio in the sequence of 2:1, 1:1, and 1:2, the amount of AuNPs deposited onto PSiNP matrices gradually increased, and the average value of Au elemental amount increased from 5.4 ± 0.1%, 9.8 ± 0.3%, to 11.4 ± 0.8%, and Si elemental amount decreased from 90.4 ± 0.5%, 87.0 ± 0.5%, to 85.0 ± 1.6%. According to the ratio between the values of the error bars and the mean, their corresponding coefficients of intrabatch variations (CV) are calculated as 1.9% (Au) and 0.6% (Si), 3.1% (Au), and 0.6% (Si), or 6.9% (Au) and 1.9% (Si), respectively. These above values of CV are less than 5%, which indicates that the growth and distribution of AuNPs on PSiNPs matrices are homogeneous at micrometer scale. Considering the deposition amount of AuNPs and their corresponding CV from EDS results, the optimized mass ratio of 1:1 was chosen to fabricate PSiNPs@Au nanocomposites with an Au loading of 44.2% (w/w) for the following experiments. Moreover, in Figure S1c (Supporting Information), Si and Au elemental concentrations of PSiNPs@Au samples were determined by inductively coupled plasma mass spectrometry (ICP-MS), indicating that the Au loading efficiency is 40.6% (w/w) close to 44.2% of EDS results. The crystalline structures of bare PSiNPs and PSiNPs@Au powders were further characterized by X-ray diffraction (XRD), recorded in Figure S1d (Supporting Information). Compared with the diffraction peaks of Si (111), (220), (311), (400), and (331) of bare PSiNPs samples, new peaks of Au (111), (200), (220), and (311) appear in PSiNPs@Au samples, indicating the growth of crystalline AuNPs onto PSiNPs. In addition, Si (111) and (220) peaks become weaken, and Si (331) peak becomes stronger, with the formation of silicon oxidation.[32] Finally, the growth of AuNPs on PSiNP matrices was also monitored by UV–vis–NIR spectra. In Figure S1e (Supporting Information), compared with bare PSiNPs, a new absorbance peak at 530 nm in PSiNPs@Au samples is attributed to the attachment of AuNPs. Overall, the homogeneous growth of AuNPs onto PSiNP matrices at micrometer scale via in situ reductive method was reported to prepare PSiNPs@Au nanocomposites in our experiments.

About 1 mL CCM solution derived from the lysates of ≈6×10^6 4T1 cancer cells regarded as its concentration of ≈6×10^6 mL^{-1} was coated onto 1 mL PSiNPs@Au solution (1 mg mL^{-1}) to create CCM@(PSiNPs@Au) nanovaccines via co-extrusion technology through a 0.8 μm polycarbonate membrane. The size, morphology, and elemental components of
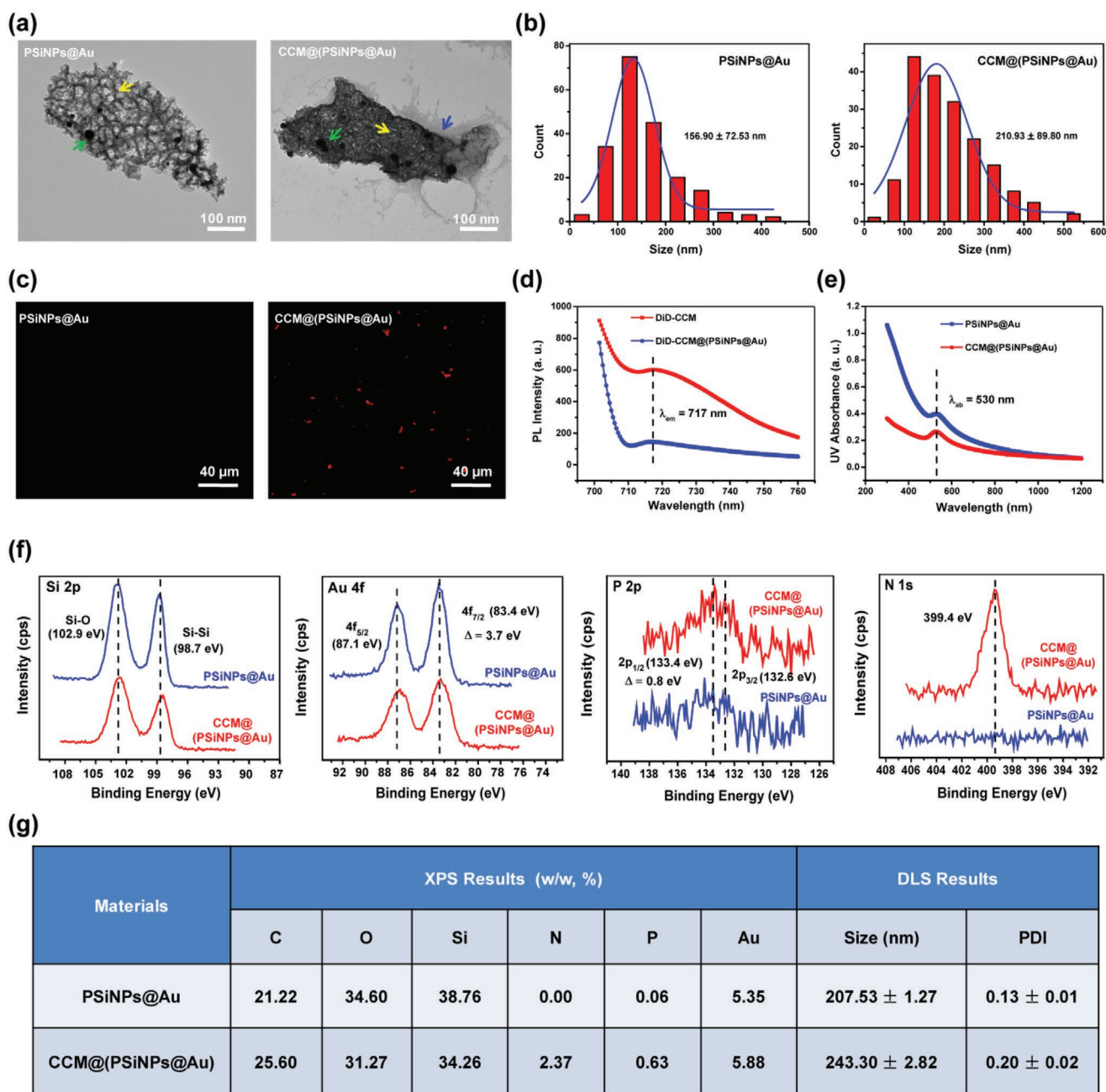
Figure 1. a) Typical TEM images; b) the size distribution results obtained from ≈200 particles; c) confocal images; d) PL spectra; e) UV–vis–NIR spectra; f) high-resolution XPS of Si, Au, P, and N elements; and g) the elemental amount and hydrodynamic sizes of PSiNPs@Au and CCM@(PSiNPs@Au) nanocomposites.

CCM, PSiNPs@Au, and CCM@(PSiNPs@Au) samples were characterized by dynamic light scattering (DLS) and transmission electron microscopy (TEM), respectively. In Figure S2a (Supporting Information), TEM results show that these opaque CCM with negative staining have inhomogeneous size distribution from hundreds of manometers to a few micrometers, and their EDS results indicate the detection of phosphorous elemental signals originated from cell membranes marked by purple circles. In **Figure 1**a and Figure S3 (Supporting Information), the nanoporous structures of PSiNPs with the size

of 10–20 nm (marked by yellow arrows) and AuNPs with the size of 15–40 nm (marked by green arrows) are clearly observed in PSiNPs@Au sample. Compared with the homogeneous distribution of AuNPs on PSiNP matrices at micrometer scale observed by SEM in Figure S1 (Supporting Information), TEM results at smaller nanometer scale show that AuNPs mainly grow on the surfaces of PSiNPs with inhomogeneous distribution. We hypothesize that the hydrophobic surfaces of hydrogen-terminated PSiNPs inhibit the deep diffusion of reactants Au^{3+} ions into their pores.

2108012 (3 of 12)

ADVANCED
SCIENCE NEWS

www.advancedsciencenews.com

ADVANCED
MATERIALS

www.advmat.de

After the encapsulation of CCM layers with negative staining (marked by blue arrows), the nanoporous structures of PSiNPs (marked by yellow arrows) and AuNPs (marked by green arrows) become blurry in the CCM@(PSiNPs@Au) sample. In addition, the size of ≈200 particles from PSiNPs@Au and CCM@(PSiNPs@Au) samples was statistically analyzed in Figure 1b. The size of PSiNPs@Au nanoparticles is 156.90 ± 72.53 nm. In contrast, the size of CCM@(PSiNPs@Au) nanoparticles increased to 210.93 ± 89.80 nm. According to DLS results in Figure 1g and Figure S4 (Supporting Information), the hydrodynamic size of PSiNPs@Au nanoparticles is 207.53 ± 1.27 nm with a polydispersity index (PDI) value of 0.13 ± 0.01 close to 0.1, indicating a good water dispersibility.[36] However, the size of CCM@(PSiNPs@Au) nanoparticles increases to 243.30 ± 2.82 nm with a PDI value of 0.20 ± 0.02. DLS results also support the aggregation of PSiNPs@Au nanoparticles induced by CCM coating, in accordance with TEM results. Here, as shown in Scheme S1c (Supporting Information), we hypothesize that during the co-extrusion process, CCM are broken into inhomogeneous fragments (step 1), and subsequently attached onto PSiNPs@Au nanoparticles via van del Waals forces (step 2), resulting in the aggregation of nanoparticles via CCM crosslinking (step 3), which is also clearly seen in Figure S3 (marked by green arrows, Supporting Information).

Elemental components of PSiNPs@Au and CCM@(PSiNPs@Au) samples were also detected by an X-ray photo-electron spectrometer (XPS) with high resolution. In Figure 1f, phosphorus elemental signal presents P $(2p_{1/2})$ and P $(2p_{3/2})$ centered at 133.4 and 132.6 eV, respectively, with a typical binding energy difference of $\Delta = 0.8$ eV, and nitrogen elemental signal presents N 1s centered at 339.4 eV. Compared with PSiNPs@Au samples, the mass amount increase of P element $(0.06\% \rightarrow 0.63\%)$ and N element $(0.00\% \rightarrow 2.37\%)$ of CCM@(PSiNPs@Au) samples is due to the introduction of protein and phospholipid compounds originated from CCM coatings. The gold elemental signal presents Au $(4f_{5/2})$ and Au $(2f_{7/2})$ centered at 88.2 and 84.5 eV, respectively, with a typical binding energy difference of $\Delta = 3.7$ eV. This result shows the successful composition of PSiNPs@Au and CCM to obtain CCM@(PSiNPs@Au) nanovaccine. For Si 2p spectra, the peak at 99.8 eV is assigned to the signal of Si—Si or Si—C, and the peak at 103.2 eV was assigned to the signal of Si—O. The results show the oxidation of Si element from PSiNPs with their reducing Au^{3+} ions to AuNPs in aqueous solution. To further investigate the interbatch reproducibility, Si and Au elemental concentrations of PSiNPs@Au and CCM@(PSiNPs@Au) samples prepared in three batches were determined by ICP-MS. In Figure S1c (Supporting Information), the average Au loading efficiency is $38.4 \pm 2.4\%$ (w/w) with the interbatch CV of 6.0% (less than 10%), showing good repeatability of samples preparation.

To qualitatively and quantitatively analyze the attachment of CCM onto PSiNPs@Au nanocomposites, (1,1-dioctadecyl-3,3,3,3-tetramethylindodicarbocyanine perchlorate (DiD) fluorescent probes are chosen due to their membrane-targeting capability. First, CCM were stained with DiD dyes to obtain DiD–CCM samples, which were characterized by confocal imaging and photoluminescent (PL) spectra. In Figure S2c (Supporting Information), confocal imaging shows that DiD–CCM

is transparent with strong red fluorescence (marked by green circles). In Figure S5a (Supporting Information), PL spectra of DiD–CCM with different concentrations show DiD characteristics emission peak at 717 nm. In Figure S5b (Supporting Information), their PL intensity at 717 nm is plotted with their corresponding concentration to obtain a good linear relationship. DiD–CCM samples were further co-extruded with PSiNPs@Au nanocomposites to prepare DiD–CCM@(PSiNPs@Au) samples. In Figure 1c and Figure S2c (Supporting Information), confocal imaging shows that red fluorescent signals of DiD-CCM are clearly observed in CCM@(PSiNPs@Au) samples, compared with PSiNPs@Au samples. A DiD characteristic peak is also observed in their corresponding PL spectra (Figure 1d). These results can also support the attachment of CCM onto PSiNPs@Au nanocomposites in our experiments. According to the standard curve method in Figure S5b (Supporting Information), the obtained ratio of CCM is calculated as $14.3 \pm 2.1\%$ after their co-extrusion with PSiNPs@Au nanocomposites. In addition, from bright channel of confocal imaging in Figure 1c, we can also find the aggregation of CCM@(PSiNPs@Au) nanoparticles, consistent with above TEM and DLS results. On this basis, UV–vis–NIR spectra of PSiNPs@Au and CCM@(PSiNPs@Au) solution were also recorded in Figure 1e. Compared with PSiNPs@Au samples, the characteristic absorbance peak of AuNPs at 530 nm still appears in CCM@(PSiNPs@Au) samples, accompanied with its intensity decreasing. This result means that the absorbance peak at 530 nm can be used to monitor the loss of PSiNPs@Au nanocomposites after co-extrusion. Accordingly, UV–vis–NIR spectra of PSiNPs@Au solution with different concentrations and their linear plot relationship were recorded in Figure S5c,d (Supporting Information). According to the same standard curve method, the obtained ratio of PSiNPs@Au is calculated as $36.6 \pm 1.2\%$. Here, considering the equal volume ratio co-extrusion of CCM solution extracted from $\approx 6 \times 10^6$ cells mL^{-1} and PSiNPs@Au solution with the concentration of 1 mg mL^{-1}, CCM@(PSiNPs@Au) nanovaccine has the equivalent concentration of $\approx 8.5 \times 10^5$ mL^{-1} CCM and 0.37 mg mL^{-1} PSiNPs@Au, that is the loading efficiency of CCM calculated as $\approx 2.3 \times 10^6$ mg^{-1}. Compared with others electrophoresis or thermogravimetric analysis technology, the quantitative method based on DiD probes developed in our experiments exhibits much higher detective sensitivity for CCM coatings, which can provide favors to monitor the reproducibility and reliability of the mass production of biomimetic nanovaccines in industry.

Cancer vaccines consisting of tumor antigens and immunostimulatory adjuvants are taken up by DCs, and then their antigens are presented to T cells, resulting in the activation of antitumor immunity in the body with cytokine secretion to specifically killing tumor cells.[28] To investigate the stimulation effect of CCM@(PSiNPs@Au) nanovaccine on antitumor immune responses in vitro, their cytotoxicity on DCs derived from the bone marrow (BMDCs) of Balb/c mice needs to be assessed in the concentration range of 0–200 μg mL^{-1}. From Figure S6 (Supporting Information), after 48 h, the viability of BMDCs co-incubated with CCM@(PSiNPs@Au) nanovaccine at the concentration of 50 μg mL^{-1} or below is $85.3 \pm 4.6\%$ or higher, and still retains $66.2 \pm 1.5\%$ at the concentration of 100 μg mL^{-1}. With the concentration increasing to 200 μg mL^{-1},

their viability sharply drops to 33.7 ± 0.4%. Accordingly, two concentrations of 50 and 100 µg mL^{-1} can be selected for next in vitro experiments. Here, PSiNPs@Au (100 µg mL^{-1}), CCM (≈1.6 × 10^6 mL^{-1}), CCM@(PSiNPs@Au) (50 µg mL^{-1}), or CCM@(PSiNPs@Au) (100 µg mL^{-1}) were first co-incubated with ≈3 × 10^5 BMDCs per well for 48 h to activate the antigen presentation of DCs. Subsequently, as-treated ≈3 × 10^5 BMDCs per well were co-cultured with ≈5 × 10^5 splenocytes derived from Balb/c mice in each well for another 48 h to stimulate the difference of T cells into CTLs. Finally, the supernatants of these cell suspensions were added into ≈1 × 10^4 4T1 tumor cells in each well for another 24 and 48 h, to assess their cytotoxic effect (**Figure 2**a). Compared with untreated 4T1 cells of group 1 as a control, the cell viability of group 2 (splenocytes + inactivated BMDCs) or group 4 (splenocytes + BMDCs activated with PSiNPs@Au) shows no significant (NS) inhibition effect on the proliferation of 4T1 cells. By contrast, the cell viability in group 3 (splenocytes + BMDCs activated with CCM), group 5 (splenocytes + BMDCs activated with 50 µg mL^{-1} CCM@(PSiNPs@Au)), and group 6 (splenocytes + BMDCs activated with 100 µg mL^{-1} CCM@(PSiNPs@Au)) significantly decrease, after 24 h (**P < 0.01) or 48 h (***P < 0.001). These results demonstrate that compared with PSiNPs@Au nanocomposites, both CCM and CCM@(PSiNPs@Au) nanovaccine can efficiently be the prime cellular immunity to kill tumor cells in vitro.

In addition, cytokines as the major mediators of adaptive immune responses can regulate the communication between APCs, lymphocytes, and other host cells.[37] However, the rapid and excessive generation of various cytokines such as interlukin-1 (IL-1), IL-6, IL-12, interferon-α (IFN-α), IFN-β, or IFN-γ, generated by the leakage of immunostimulatory adjuvants, can induce acute respiratory distress syndrome and multiple organ failure.[19] Accordingly, the secretion of IFN-γ as a pro-inflammation cytokine was analyzed during the co-culture period of BMDCs and splenocytes, recorded in Figure 2b. Compared with group 1 (splenocytes + inactivated BMDCs) as a control, group 2 activated with PSiNPs@Au, and group 3 activated with CCM, the concentration of IFN-γ secretion in group 4 activated with CCM@(PSiNPs@Au) significantly increase to 45.7 ± 7.2 pg mL^{-1} (***P < 0.001), even after 24 h. With time prolonging to 48 or 72 h, the secretion of IFN-γ also happens in group 2 or 3. However, compared with the high IFN-γ secretion from BMDCs activated oxidized PSiNPs (>500 pg mL^{-1}) or hydrocarbonized PSiNPs (>200 pg mL^{-1}) with a low concentration of 25 µg mL^{-1} reported in our previous studies,[28] PSiNPs@Au nanocomposites with a much higher concentration of 100 µg mL^{-1} only produce less than 80 pg mL^{-1} of IFN-γ, indicating their weak immunostimulatory effect on immune cells to generate cytokines. From XPS results, the oxidation of PSiNPs originated from PSiNPs@Au nanocomposites also happen with the reductive synthesis of surface attached AuNPs. Considering that the immunostimulatory effect of PSiNPs is strongly dependent on their surface chemistry, the strong intrinsic immunostimulatory effect generated by oxidized PSiNP
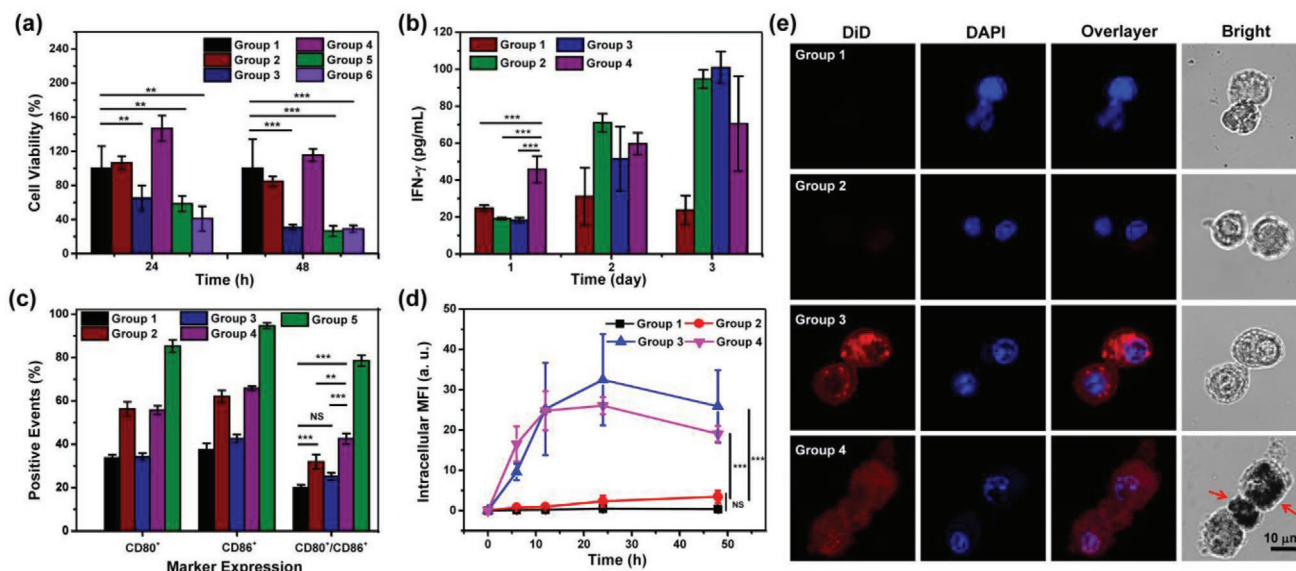

Figure 2. a) Cell viability of untreated 4T1 cells as control group 1, and 4T1 cells treated with splenocytes + inactivated BMDCs as group 2, splenocytes + BMDCs activated with CCM as group 3, splenocytes + BMDCs activated with PSiNPs@Au as group 4, or splenocytes + BMDCs activated with CCM@(PSiNPs@Au) (50 µg mL^{-1}) as group 5, (100 µg mL^{-1}) as group 6 (n = 4 biologically independent samples). b) IFN-γ secretion of splenocytes + inactivated BMDCs as group 1, splenocytes + BMDCs activated with CCM as group 2, splenocytes + BMDCs activated with PSiNPs@Au as group 3, and splenocytes + BMDCs activated with CCM@(PSiNPs@Au) as group 4 (n = 2 biologically independent samples). c) The expression of CD80, CD86, and CD80/CD86 signals of inactivated BMDCs as negative control group 1, and BMDCs activated with CCM as group 2, with PSiNPs@Au as group 3, with CCM@(PSiNPs@Au) nanovaccine as group 4, or with LPS as positive control group 5 (n = 3 biologically independent samples). d) The relationship between intracellular MFI intensity and co-culture time (n = 100 biologically independent samples). e) Confocal images of untreated BMDCs as group 1, co-incubated with DiD–CCM (≈1.2 × 10^5 cells mL^{-1}) as group 2, DiD–CCM (≈8.4 × 10^5 cells mL^{-1}) as group 3, and CCM@(PSiNPs@Au) nanovaccine (50 µg mL^{-1}) as group 4. The error bars are based on standard errors of the mean (***P < 0.001, **P < 0.01, or NS P > 0.05 by analysis of variance (ANOVA) with Tukey's post-test).

**ADVANCED
SCIENCE NEWS**

www.advancedsciencenews.com

**ADVANCED
MATERIALS**

www.advmat.de

components of PSiNPs@Au nanocomposites is significantly attenuated by plenty of surface-attached AuNPs with a strong immunosuppressive effect on DCs.[38]

The antigen presentation of DCs activated with cancer vaccines is the initial step of adaptive immunity, which can determine their immunotherapeutic efficacy.[39] Thus, the co-stimulatory CD80/CD86 expression of DCs as an important antigen presenting biomarker was monitored in our experiments. First, lipopolysaccharide (LPS, 100 µg mL^{-1}), PSiNPs@Au (100 µg mL^{-1}), CCM ($\approx 1.6 \times 10^6$ mL^{-1}), or CCM@(PSiNPs@Au) (100 µg mL^{-1}) were co-incubated with $\approx 3 \times 10^5$ BMDCs per well for 48 h. Subsequently, these cell samples were stained with fluorescently labeled antibodies to evaluate their co-expression of CD80/CD86 signals. Group 1 of untreated BMDCs is used as a negative control for characterizing, and group 5 of LPS is used as the positive control due to its efficient upregulation of CD80/CD86 expression. In Figure 2c and Figure S7 (Supporting Information), the co-expression of CD80/CD86 signals (25.1 ± 1.7%) of BMDCs activated with PSiNPs@Au samples from group 3 is only 25.1 ± 1.7% with no significant differences ($P > 0.05$), compared with 19.9 ± 1.4% of negative control group 1. This result shows that PSiNPs@Au nanocomposites have negligible stimulation on the antigen presentation of DCs. By contrast, bare CCM of group 2 efficiently activated BMDCs with CD86/CD80 co-expression increasing to 31.9 ± 3.4% (***$P < 0.001$). Similar phenomena of that CCM or CCM-based vesicles not only provide tumor antigens, but also activate immune cells have ever been reported.[29,40,41] With CCM coating onto PSiNPs@Au nanoparticulate cores to obtain CCM@(PSiNPs@Au) nanovaccine (group 4), it can stimulate BMDCs with the higher CD86/CD80 co-expression of 42.6 ± 2.5% (***$P < 0.001$). Considering that equivalent CCM concentration ($\approx 2.3 \times 10^5$ mL^{-1}) of CCM@(PSiNPs@Au) nanovaccine in group 4 is much lower than that ($\approx 1.6 \times 10^6$ mL^{-1}) of CCM in group 2, these attached CCM have an enhanced immunostimulatory effect on antigen presentation of DCs, compared with free CCM.

To explore the mechanism of this enhanced immunostimulatory effect, the uptake of DiD–CCM by DCs was monitored at different time points by confocal imaging. Here, $\approx 3 \times 10^5$ BMDCs alone are cultured for 48 h as control group 1, co-cultured with DiD–CCM ($\approx 1.2 \times 10^5$ mL^{-1}) as group 2, DiD–CCM ($\approx 8.4 \times 10^5$ mL^{-1}) as group 3, and DiD–CCM@(PSiNPs@Au) nanovaccine (50 µg mL^{-1}) as group 4. In Figure 2e, the red fluorescent signals generated from DiD probes inserted in CCM are used to detect CCM uptake by DCs, combined with the blue fluorescent signals from 4′,6-diamidino-2-phenylindole (DAPI) probes targeting intracellular nuclei. Compared with control group 1, strong red fluorescent signals are obviously observed in group 3, but no fluorescent signals appear in group 2 after 24 h culture. The result indicates that the internalization of DiD–CCM into DCs is strongly dependent on their concentration. However, by comparing group 2 with group 4 with the same low-equivalent DiD–CCM concentration, their uptake efficiency can be significantly enhanced using PSiNPs@Au nanocomposites as carriers. From the bright channel in Figure 2e, it is clearly observed that exogenous PSiNPs@Au nanocomposites can efficiently accumulate inside DCs (marked by red arrows), recognized as "foreign bodies."[42,43] Moreover, the mean fluorescent intensity (MFI) from ≈ 100 cells is further calculated to

track the kinetics changes of DiD–CCM concentrations inside DCs during 48 h, recorded in Figure 2d. Compared with control group 1, DiD–CCM uptake in group 2 is negligible after 48 h. By contrast, intracellular CCM amount of groups 3 and 4 is much higher than that of group 2 with the significant difference of ***$P < 0.001$. Notably, in group 3 or 4, intracellular CCM concentration sharply increases during first 24 h, due to DiD–CCM uptake by DCs. However, a gradual decrease happens in next 24 h, indicating the digestion of DiD–CCM by DCs accompanied with the release of the inserted DiD probes with strong fluorescence into free ones with no fluorescence. According to these abovementioned results, exogenous PSiNPs@Au nanocomposites can efficiently deliver their surface-coated CCM into DCs to enhance their intracellular concentration, compared with endogenous CCM alone. In addition, protein-based tumor antigens from these internalized CCM with higher concentration can be digested into more epitopic peptide fragments to be cross-presented by DCs, which results in an enhanced immunostimulatory effect of CCM@(PSiNPs@Au) nanovaccine on the activation of antigen-specific antitumor immunity to kill more tumor cells.[43] As far as we know, this strategy that biomimetic nanovaccine based on weak-immunostimulatory nanoparticulate cores has never been reported, which can still efficiently boost antitumor immunity. In addition, this nanovaccine based on endogenous CCM coatings and nanoparticulate cores with weak immunostimulatory effect can also control the excessive secretion of cytokines from immune cells to avoid the high risk of systematic inflammation, which is favorable for its future clinical applications.

Recently, PSiNPs@Au nanocomposites have been used as photothermal agents to kill cancer cells and thermally ablate tumors.[32–35,44] Here, to test the photothermal effect of PSiNPs@Au and CCM@(PSiNPs@Au) nanocomposites dispersed in deionized (DI) water, a thermal imaging camera was used to measure their temperature changes during 808 nm laser irradiation with the power intensity of 1.6 W cm^{-2}. In **Figure 3**a, after 10 min exposure upon near-infrared (NIR) laser irradiation, the temperature of 200 µg mL^{-1} PSiNPs@Au suspension remarkably increases with $\Delta T = 24.8$ °C. By contrast, the temperature of DI water shows negligible changes ($\Delta T = 4.2$ °C) under the same condition. Compared with PSiNPs@Au suspension alone, ΔT of CCM@(PSiNPs@Au) suspension slightly decreases to 19.1 °C, because CCM coating can block the absorbance of NIR laser. In Figure 3b,c, the photothermal effect of CCM@(PSiNPs@Au) suspension is dependent on their concentration and NIR laser power. To investigate the stability of the photothermal effect, 200 µg mL^{-1} of PSiNPs@Au solution was also irradiated with 1.6 W cm^{-2} NIR laser for 10 min (Laser ON), followed by turning off the laser irradiation (Laser OFF) and cooling down to room temperature. In Figure 3d, 16.7, 16.9, and 17.9 °C of ΔT are recorded after sequential cycles, indicating the slight recovery of the photothermal effect upon the repeated exposure of NIR laser. To investigate the stability of CCM coatings under NIR irradiation, 200 µg mL^{-1} of DiD–CCM@(PSiNPs@Au) samples was used to be irradiated with NIR laser (1.6 W cm^{-2}, 10 min), and then observed by confocal imaging in Figure 3e. Compared with CCM@(PSiNPs@Au) samples without NIR irradiation, their red fluorescent signals become much weaker
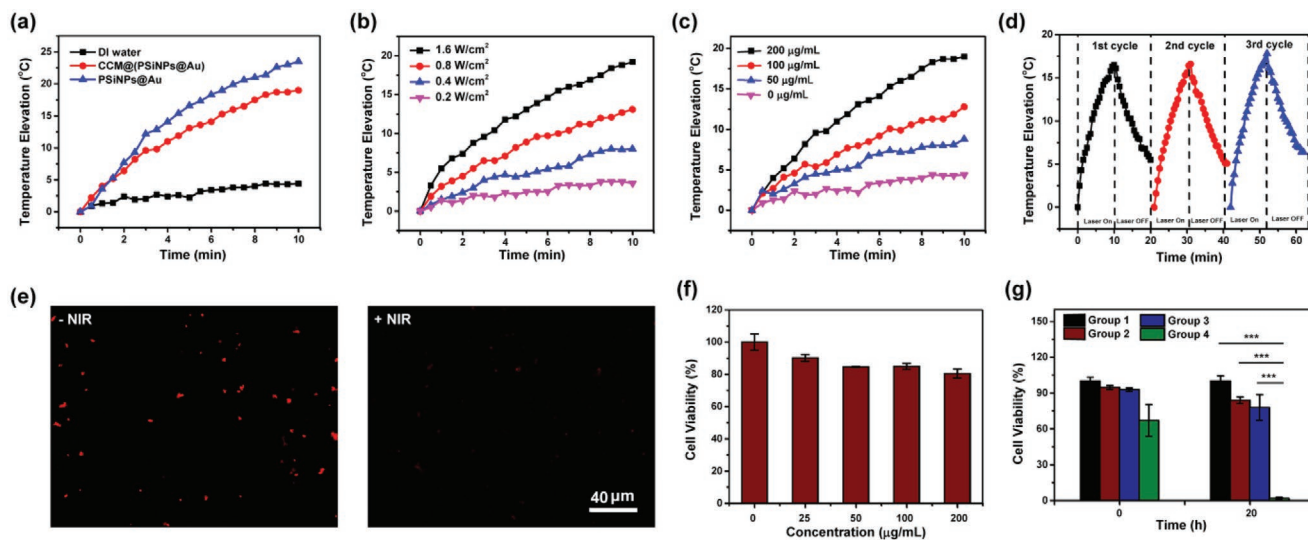
Figure 3. a) Temperature elevation of 200 µg mL^{-1} CCM@(PSiNPs@Au), 200 µg mL^{-1} PSiNPs@Au, and DI water with 10 min exposure of 808 nm laser irradiation with the power intensity of 1.6 W cm^{-2}. b) Temperature elevation of 200 µg mL^{-1} CCM@(PSiNPs@Au) under 10 min NIR laser irradiation with different power intensity. c) Temperature elevation of CCM@(PSiNPs@Au) at different concentrations under 10 min NIR laser irradiation with the power intensity of 1.6 W cm^{-2}. d) Temperature elevation of 200 µg mL^{-1} CCM@(PSiNPs@Au) with three cycles of "Laser ON" and "Laser OFF." e) Confocal imaging of 200 µg mL^{-1} CCM@(PSiNPs@Au) with or without 10 min NIR laser irradiation. f) Cell viability of 4T1 cells incubated with CCM@(PSiNPs@Au) with different concentrations for 6 h culture ($n = 3$ biologically independent samples). g) The viability of untreated 4T1 cells as control group 1, and 4T1 cells irradiated with 1.6 W cm^{-2} NIR laser for 10 min as group 2 (4T1 + NIR), co-incubated with 200 µg mL^{-1} CCM@(PSiNPs@Au) without NIR laser irradiation as group 3 (4T1 + vaccine), and co-incubated with 200 µg mL^{-1} CCM@(PSiNPs@Au) irradiated with 1.6 W cm^{-2} NIR laser for 10 min as group 4 (4T1 + vaccine + NIR) ($n = 4$ biologically independent samples). The error bars are based on standard errors of the mean (***$P < 0.001$, by ANOVA with Tukey's post-test).

upon the exposure of NIR irradiation, resulted from the release of DiD probes from CCM layers. Combined with TEM images in Figure S2b (Supporting Information), the integrate structures of CCM are destroyed with NIR irradiation, resulting in the formation of the nanovesicles. In addition, DLS results also showed that the hydrodynamic size of CCM@(PSiNPs@Au) under NIR irradiation reduces by ≈18 nm, due to the disintegration of CCM crosslinking induced by NIR irradiation. These results indicate that local high temperature generated by the photothermal effect of PSiNPs@Au nanoparticulate cores can break the integrated structures of their encapsulated CCM layers, resulting in the recovery of their photothermal effect.

To study the photothermal therapy of cancer cells, the cell viability of 4T1 cells co-incubated with CCM@(PSiNPs@Au) nanovaccine at different concentrations was assessed in Figure 3f. The results show that even at the highest concentration (200 µg mL^{-1}) of materials, the cell viability of 4T1 cells is still higher than 80%. Here, 200 µg mL^{-1} of CCM@(PSiNPs@Au) nanovaccine was selected to be co-incubated with 1×10^4 4T1 cells per well under NIR laser irradiation for 10 min, and then the cell viability was immediately assessed (Figure 3g). Compared with group 1 (untreated 4T1 cells) as a control, the cell viability of group 2 (4T1 + NIR) or group 3 (4T1 + vaccine) shows negligible changes. In contrast, the cell viability of group 4 (4T1 + vaccine + NIR) decreases to 66.9 ± 13.4%. As time prolonging to 20 h, a higher inhibitive efficiency (1.69 ± 1.0%, ***$P < 0.001$) is obtained in group 4, compared with the other groups. These results demonstrate that CCM@(PSiNPs@Au) nanovaccine as a photothermal agent has a significant photothermal therapeutic efficacy for tumor cells.

The activation of CCM@(PSiNPs@Au) nanovaccine on the antitumor immunity to prevent the occurrence of solid tumors was further investigated in vivo. Here, with the day of tumor inoculation defined as day 0, the total experimental process is divided into two stages (**Figure 4**a): 1) vaccination and biosafety evaluation (from day −29 to day −1 before tumor inoculation); and 2) tumor inoculation and the observation of tumor growth and long-term survival (days 0–55 after tumor inoculation). In stage (1) on days −29, −26, −22, and −8, 68 female Balb/c mice with the age of 4–5 weeks were randomly divided into four groups with repeated subcutaneous injection near the inguinal lymph nodes (LNs) of their left hind legs, including the injection of physiological saline as a control group 1, PSiNPs@Au suspension as particle group 2, CCM solution as CCM group 3, and CCM@(PSiNPs@Au) suspension as vaccine group 4. In stage (1), on day −1 before tumor inoculation, tissue sections of heart, liver, spleen, lung, and kidney were also prepared for pathological analysis via hematoxylin–eosin (H&E) staining (Figure 4b). Compared with the control group 1, no pathological lesions are observed in groups 2–4. In addition, during 28 days in stage (1), the body weight of the mice was measured every 3 days (Figure 4c). The curves from groups 2–4 are close to that of the control group 1, indicating no toxicity affecting the growth of vaccinated mice. From complete blood panel and serum biochemistry analysis in Figure S8 (Supporting Information), compared with control group 1, no obvious changes are also observed in groups 2–4, which are in or close to the reference range of healthy female Balb/c mice. These results further demonstrate that the CCM@(PSiNPs@Au) nanovaccine composed of endogenous CCM coatings, and
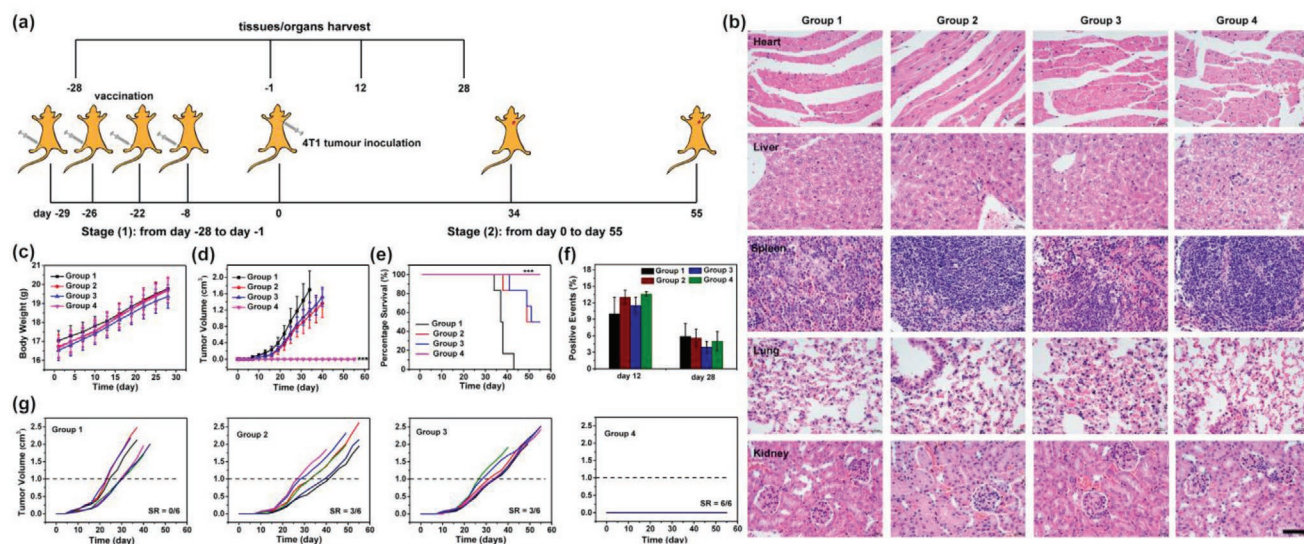
ADVANCED
SCIENCE NEWS
www.advancedsciencenews.com

ADVANCED
MATERIALS
www.advmat.de

Figure 4. a) Schematic of the in vivo vaccination experiments. b) H&E staining of tissue section including heat, liver, spleen, lung, and kidney of the sacrificed mice randomly chosen from all groups on day −1 (scale bar = 40 μm). c) Body weight of the mice from all groups during 28 days in stage (1) (*n* = 15 biologically independent samples). d) The average 4T1 tumor growth curves from all groups in stage (2) (*n* = 6 biologically independent samples). e) Survival percentage of the mice from all groups in stage (2) (*n* = 6 biologically independent samples). f) The co-expression of CD3/CD8 signals of T cells derived from spleens of the mice from all groups on day 12 or 28 (*n* = 3 biologically independent samples). g) The individual 4T1 tumor growth curves from groups. Here, the injection of physiological saline as a control group 1, PSiNPs@Au suspension as particle group 2, CCM solution as CCM group 3, and CCM@(PSiNPs@Au) suspension as vaccine group 4. The error bars are based on standard errors of the mean (***P < 0.001 by ANOVA with Tukey's post-test, and log-rank (Mantel–Cox) test for survival analysis, in comparison of group 5 and the other groups).

weak-immunostimulative PSiNPs@Au nanoparticulate cores have good biosafety without the risk of acute and heavy systematic inflammation. Furthermore, on day 0, ≈1 × 10^5 of 4T1 cells were subcutaneously implanted near the armpit of the right forelimbs of 12 vaccinated mice in groups 1–4. During the next 28 days in stage (2), the volume of 4T1 tumor in groups 1–4 was measured every 3 days (Figure 4d,g). Compared with the average volume of 4T1 tumors from control group 1, particle group 2, and CCM group 3, no occurrence of 4T1 tumors from vaccine group 4 is observed (***P < 0.001). Even without other immunotherapeutic treatments until day 55, no occurrence of 4T1 tumors in group 4 is observed. In addition, the weight of the tumors extracted from the sacrificial mice on day 28 was also recorded in Figure S9 (Supporting Information), in accordance with the results of tumor volume. During long-term survival observation until day 55, the survival curves of the mice from all groups are presented in Figure 4e. Compared with the survival rate of control group 1 (0%), particle group 2 (50%), and CCM group 3 (50%), all immunized mice of vaccine group 4 survive (***P < 0.001). The results show that CCM@(PSiNPs@Au) nanovaccine has a good prophylactic efficacy on the occurrence of solid tumors, resulting in the survival of the immunized mice.

To investigate the mechanism of immune responses stimulated by CCM@(PSiNPs@Au) nanovaccine in the body, on day −28 in stage (1), two mice were randomly chosen and sacrificed to extract cell populations from spleens, which were used to test co-expression of CD80/CD86 signals of DCs. In Figures S10a and S11a (Supporting Information), CD80/C86 co-expressions of particle group 2 (5.0 ± 2.9%) and CCM group 3 (3.3 ± 0.8%) have no significant differences with that (4.5 ± 0.0%) of the control group 1. The results show that PSiNPs@Au

nanocomposites still have no significant immunostimulatory effect on DCs in vivo, in accordance with above in vitro experimental results (Figure 2a). By contrast, even at the same high concentration of in vitro experiments, CCM unsuccessfully activate DCs under in vivo conditions. However, with CCM attached onto exogenous PSiNPs@Au nanocomposites to obtain CCM@(PSiNPs@Au) nanovaccine, it can efficiently activate DCs with much higher co-expression lever (12.6 ± 0.9%) of CD80/C86 signals in the body. In addition, memory lymphocytes like effector memory T cells (T$_{EM}$, CD44$^+$/CD62L$^-$) and central memory T cells (T$_{CM}$, CD44$^+$/CD62L$^+$) can provide immediate protection in peripheral tissues and mount recall responses to antigens in secondary lymphoid organs.[45] Accordingly, two randomly vaccinated mice from all groups were sacrificed on day −1, and cell populations were extracted from the spleens to test the co-expression of CD44/CD62L of CD8$^+$ CTLs (Figures S10b,c and S11b, Supporting Information). The co-expression level of CD44$^+$/CD62L$^+$ or CD44$^+$/CD62L$^-$ is the highest in vaccine group 4 (12.7 ± 8.4% or 3.8 ± 1.3%), compared with control group 1 (5.9 ± 2.2% or 1.9 ± 1.9%), particle group 2 (1.8 ± 1.0% or 2.0 ± 0.7%), and CCM group 3 (2.9 ± 2.5% or 3.0 ± 0.7%). This result indicates the success establishment of an immune memory state via the differentiation of T cells induced by CCM@(PSiNPs@Au) nanovaccine. Moreover, on day 12 or 28 in stage (2), three mice were randomly chosen and sacrificed, and cell populations were extracted from their spleens to test the co-expression of CD3/CD8 of T cells. In Figure 4f and Figure S12 (Supporting Information), the co-expression level of CD3/CD8 signals (13.6 ± 0.4%) from vaccine group 4 is the highest on day 12, compared with that of groups 1–3. The result supports that CD8$^+$ CTLs activated by CCM@(PSiNPs@Au) nanovaccine efficiently prevent the

occurrence of 4T1 tumors. As time prolonging to day 28, the positive events of CD3/CD8 from vaccine group 4 drop to 5.0 ± 1.8%, respectively, close to the level (5.8 ± 2.4%) of the control group 1. The results indicate that after 28 days post tumor inoculation, the antitumor immune responses activated by CCM@(PSiNPs@Au) nanovaccine are completely attenuated.[46] In previous studies,[17] nanovaccines with the diameter size of >100 nm, they cannot directly go into lymphatic capillary from interstitium via subcutaneous injection. Instead, they need be internalized with DCs and then migrate into the LNs to activate immune responses. Combined with the above in vitro results (Figure 2), endogenous CCM alone with size range of hundreds of manometers to a few micrometers difficultly recruit DCs to uptake them in the body, resulting in the failure of the activation of antitumor immunity. However, with the help of foreign body responses, exogenous PSiNPs@Au nanocomposites with the size of 243.30 ± 2.82 nm can efficiently recruit DCs to deliver CCM into them and activate them. These activated DCs continue to migrate into LNs to induce the differentiation of naive T cells into CD8$^+$ CTLs, CD44$^+$/CD62L$^-$ T$_{EM}$, and CD44$^+$/CD62L$^+$ T$_{CM}$ to trigger antigen-specific antitumor immunity followed with the establishment of an immune memory state, resulting in no occurrence of solid tumors and the survival of all vaccinated mice during 55 day observation.

To investigate the combined photothermal–immunotherapeutic efficacy based on CCM@(PSiNPs@Au) nanovaccine as a photothermal agent against established solid tumors, in vivo experiments were also carried out. When the day of photothermal therapy was defined as day 0, the total experimental process is divided into two stages (**Figure 5**a): 1) bilateral tumors inoculation (day −10 to day −1 before photothermal therapy) and 2) combined photothermal immunotherapy, and the observation of tumor growth and long-term survival (days 0–45 after photothermal therapy). In stage (1), on day −10, ≈1 × 10^6 of 4T1 cells were subcutaneously implanted in the lateral of the right hind limbs of female Balb/c mice with the age of 4–5 weeks to inoculate primary solid tumors. On day −3, another ≈1 × 10^6 of 4T1 cells were subcutaneously implanted in the lateral of the left hind limbs of these mice to inoculate distal tumors to obtain metastatic tumor model. In stage (2), 80 mice bearing the metastatic tumor model were randomly divided into five groups, including group 1 as a control, group 2 (NIR + ICB), group 3 (NIR + vaccine), group 4 (vaccine + ICB), and group 5 (NIR + vaccine + ICB). For control group 1 and group 2 (NIR + ICB), physiological saline was intratumorally injected into primary tumors of mice, and CCM@(PSiNPs@Au) suspension was administrated into mice of groups 3–5 by the same way. Subsequently, 1.6 W cm^{-2} NIR laser was immediately irradiated on the primary tumors from groups 2, 3, and 5. The elevated temperature of these irradiated tumors was monitored by thermal imaging (Figure 5b; Figure S13, Supporting Information). The results demonstrate that, without NIR irradiation, no significant temperature elevation appears in control group 1 or group 4, followed by the slight decrease of body temperature. In the presence of NIR laser irradiation, the temperature increases from 26.4 to 52.2 °C in group 3, and from 26.7 to 54.4 °C in group 5, due to the photothermal effect of CCM@(PSiNPs@Au) nanovaccine. Even without the injection of photothermal agents, the temperature of tumor site in group 2 still increases

from 27.8 to 39.4 °C under the same irradiation, resulted from the self-heating of tissues irradiated by NIR laser.[25] Finally, on days 1, 4, and 7 in stage (2), the anti-CTLA-4 antibody solution was intraperitoneally injected in as-treated mice in groups 2, 4, and 5 for ICB immunotherapy. The volume of primary and distal tumors from groups 1–5 was recorded every 2 days post photothermal therapy. In Figure 5c,h, after 10 days, the growth of tumors stops in group 5. By contrast, the tumors from groups 1–4 continue to grow. After 25 days post photothermal therapy, an average tumor volume (0.6 ± 0.1 cm^3) of group 5 is the lowest (***P < 0.001), compared with control group 1 (2.1 ± 0.3 cm^3), group 2 (1.3 ± 0.2 cm^3), group 3 (1.0 ± 0.2 cm^3), and group 4 (1.8 ± 0.3 cm^3). Moreover, Figure 5d,i records the average volume of distal tumors from groups 1 to 5. The results show that the occurrence of distal tumors appears in control groups 1 and 4. However, no occurrence of distal tumors is found in groups 2, 3, and 5. Figure 5e shows the survival curves of the mice from all groups until day 45. Compared with the survival rate (0%) from control groups 1 and 4, all mice from groups 2, 3, and 5 survive (****P < 0.001). Here, these five groups are divided into two types: 1) with NIR laser treatment including groups 2, 3, and 5 and 2) without NIR laser treatment, including control groups 1 and 4. It is obviously found that photothermal therapy can efficiently inhibit the growth of primary solid tumors and the occurrence of distal metastatic tumors, leading to 100% survival rate of the treated mice. Even no injection of photothermal agents in group 2 also improves the survival rate of mice due to their mild photothermal effect. Although the therapeutic efficacy of groups 2 and 3 on the survival and metastasis is the same with that of group 5 during the short observation periods of 45 days, it is expected more death of the mice in groups 2 and 3 overtime due to the growth of their residual primary tumors. Therefore, photothermal therapy synergized immunotherapy based on CCM@(PSiNPs@Au) nanovaccine as a photothermal agent shows the best therapeutic efficacy on the growth and metastasis of established solid tumors, considering the whole inhibitive effect on primary and distal tumors.

To further explore the mechanism of this combination therapy, three random mice were sacrificed on day 3. Cell populations were extracted from their spleens to test the co-expression of CD80/CD86 of DCs and from their tumors to test the co-expression of CD3/CD8 of T cells. Figure 5f and Figure S14 (Supporting Information) show that the co-expression level of CD80/CD86 signals from group 5 significantly increases (***P < 0.001), compared with the others groups 1–4. Figure 5g and Figure S15 (Supporting Information) show that the co-expression level of CD3/CD8 (41.9 ± 18.4%) from group 5 is also the highest, compared with control group 1 (13.5 ± 12.3%), group 2 (30.6 ± 13.3%), group 3 (32.6 ± 18.6%), and group 4 (17.7 ± 8.3%). Moreover, on day 9, three random mice were sacrificed, and cell populations were also extracted from their inguinal LNs near tumor sites to test the co-expression of CD3/CD8 signals of T cells. Figure 5g and Figure S16 (Supporting Information) show that the CD3/CD8 co-expression of T cells from group 5 (19.4 ± 5.0%) is upregulated, compared with control group 1 (5.5 ± 5.1%), group 2 (13.1 ± 4.9%), group 3 (8.6 ± 7.2%), and group 4 (6.5 ± 2.6%). Here, these five groups can be also divided into types with or without NIR laser as
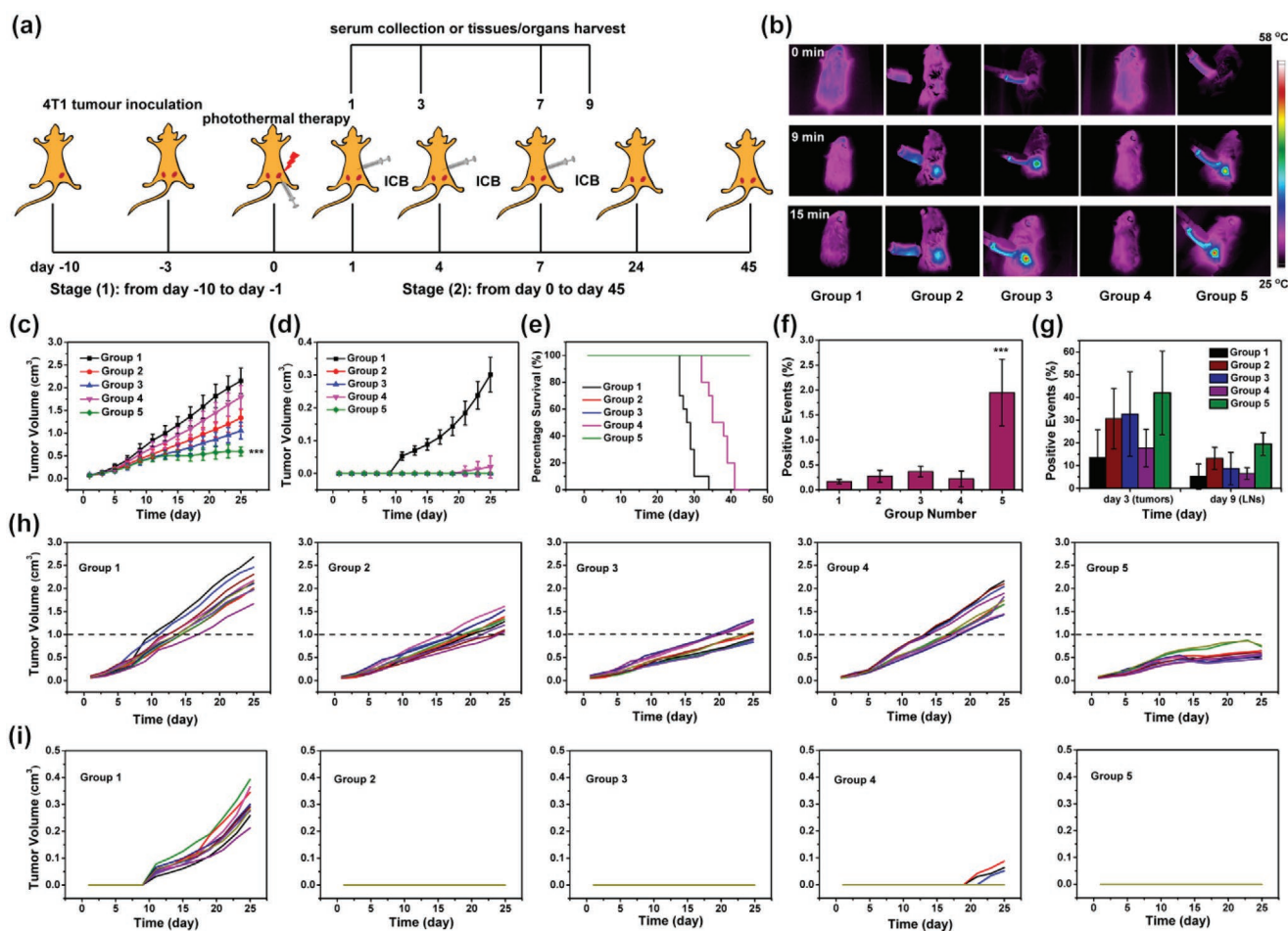
Figure 5. a) Schematic route of in vivo combined photothermal–immunotherapy experiments. b) Thermal imaging of the mice from all groups irradiated by 1.6 W cm^{-2} NIR laser for 15 min. c) The average size curves of primary 4T1 tumors from all groups in stage (2) ($n = 10$ biologically independent samples). d) The average size curves of distal 4T1 tumors from all groups in stage (2) ($n = 10$ biologically independent samples). e) Survival percentage of the mice from all groups in stage (2) ($n = 10$ biologically independent samples). f) The co-expression of CD80/CD86 signals of DCs derived from spleens on day 3 from all groups ($n = 3$ biologically independent samples). g) The co-expression of CD3/CD8 signals of T cells derived from tumors on day 3, or LNs on day 9 from all groups ($n = 3$ biologically independent samples). h,i) The individual size curves of primary 4T1 tumors (h) and distal 4T1 tumors (i) from all groups in stage (2). Here, group 1 as a control, group 2 (NIR + ICB), group 3 (NIR + vaccine), group 4 (vaccine + ICB), and group 5 (NIR + vaccine + ICB). The error bars are based on standard errors of the mean (***$P < 0.001$ by ANOVA with Tukey's post-test, and log-rank (Mantel–Cox) test for survival analysis, in comparison of group 5 and the other groups).

described above. The infiltration of CD8$^+$ CTLs in tumor sites, the activation of DCs in spleen, and the recruitment of CD8$^+$ CTLs in LNs near tumor sites are also found to be dependent on photothermal therapy. This is because photothermal therapy can destroy dense extracellular matrix and accelerate blood circulation of solid tumor to improve the infiltration of CD8$^+$ CTLs in solid tumors, which can sensitize solid tumors for ICB immunotherapy.[24,47] In addition, photothermal therapy can also activate the immune cells in the body to elicit antitumor immunity, leading to no occurrence of distal tumors. Considering the denaturization of protein-based tumor antigens from CCM@(PSiNPs@Au) nanovaccine induced by local high temperature (Figure 3e), the activation of immune responses is attributed to the antigen release of heat-damaged tumor cells initiated by photothermal therapy.[23] Finally, the fundus blood was repeatedly collected from the mice of all groups on days 1, 3, and 7, for the quantification analysis of cytokines secretion

including IL-6, IL-10, tumor necrosis factor-α (TNF-α), and IFN-γ, as shown in Figure S17 (Supporting Information). Considering that IL-6 as pro-inflammation cytokine is involved in Th2 immune response and promote immune responses,[37] the secretion level of groups 2, 3, and 5 with NIR irradiation is higher than that from groups 1 and 4 without NIR irradiation on day 1. Moreover, IL-6 secretion from group 5 is still at high level on day 3, and drops to the lowest lever on day 7. IL-10 secretion as anti-inflammatory cytokines from group 5 is the highest on day 1, and it also drops to the lowest lever on day 7. For TNF-α as pro-inflammation cytokine to enhance the difference and activation of DCs or T cells,[37] similar changes are also observed. As for IFN-γ, no significant differences appeared among these five groups from days 1 to 7. These results demonstrate that photothermal therapy can produce local inflammatory responses in irradiated tumor sites on day 1, with the secretion of inflammation cytokines such as TNF-α, IL-6, or

IL-10.[24,48–50] With the suppression of local inflammation, their secretion significantly subsides on day 7. Among them, pro-inflammation factors including TNF-α and IL-6 can efficiently reverse immunosuppressive TME, to enhance the efficacy of photothermal therapy synergized with immunotherapy.[23] Overall, photothermal therapy based on CCM@(PSiNPs@Au) nanovaccine can not only directly destroy the established solid tumors, but also induce local inflammations to sensitize solid tumors for additional immunotherapies.

3. Conclusions

A CCM@(PSiNPs@Au) nanovaccine based on weak-immunostimulatory PSiNPs@Au nanoparticulate cores with the loading efficiency ($\approx$2.3 $\times$ 10^6 mg^{-1}) of CCM has been reported. This nanovaccine with good biosafety can boost the antitumor immunity to prevent the occurrence of solid tumors, resulting in the survival of all immunized mice. Combined with ICB immunotherapy, the CCM@(PSiNPs@Au) nanovaccine can be also used as photothermal agents to eliminate the established solid tumors and suppress their metastasis, via the initiation of the antitumor immune responses in the body and the reversion of their immunosuppressive microenvironments. Therefore, this strategy is important to develop multifunctional nanovaccines with better biosafety and more diagnosis or therapeutic modalities against the occurrence, recurrence, or metastasis of solid tumors in future.

Supporting Information

Supporting Information is available from the Wiley Online Library or from the author.

Acknowledgements

Conflict of Interest

The authors declare no conflict of interest.

Data Availability Statement

The data that support the findings of this study are available from the corresponding author upon reasonable request.

Keywords

[1] K. Palucka, H. Ueno, J. Banchereau, *J. Immunol.* **2011**, *186*, 1325.
[2] D. S. Chen, I. Mellman, *Immunity* **2013**, *39*, 1.
[3] Z. Hu, P. A. Ott, C. J. Wu, *Nat. Rev. Immunol.* **2018**, *18*, 168.
[4] Y. Fan, J. J. Moon, *Vaccines* **2015**, *3*, 662.
[5] R. S. Riley, C. H. June, R. Langer, M. J. Mitchell, *Nat. Rev. Drug Discovery* **2019**, *18*, 175.
[6] A. J. Najibi, D. J. Mooney, *Adv. Drug Delivery Rev.* **2020**, *161–162*, 42.
[7] S. Liu, Q. Jiang, X. Zhao, R. Zhao, Y. Wang, Y. Wang, J. Liu, Y. Shang, S. Zhao, T. Wu, Y. Zhang, G. Nie, B. Ding, *Nat. Mater.* **2021**, *20*, 421.
[8] J. Xu, J. Lv, Q. Zhuang, Z. Yang, Z. Cao, L. Xu, P. Pei, C. Wang, H. Wu, Z. Dong, Y. Chao, C. Wang, K. Yang, R. Peng, Y. Cheng, Z. Liu, *Nat. Nanotechnol.* **2020**, *15*, 1043.
[9] N. Gong, Y. Zhang, X. Teng, Y. Wang, S. Huo, G. Qing, Q. Ni, X. Li, J. Wang, X. Ye, T. Zhang, S. Chen, Y. Wang, J. Yu, P. C. Wang, Y. Gan, J. Zhang, M. J. Mitchell, J. Li, X. Liang, *Nat. Nanotechnol.* **2020**, *15*, 1053.
[10] P. G. Lokhov, E. E. Balashova, *J. Cancer* **2010**, *1*, 230.
[11] A. V. Kroll, Y. Jiang, J. Zhou, M. Holay, R. H. Fang, L. Zhang, *Adv. Biosyst.* **2019**, *3*, 1800219.
[12] R. H. Fang, A. V. Kroll, W. Guo, L. Zhang, *Adv. Mater.* **2018**, *30*, 1706759.
[13] M. Xuan, J. Shao, J. Li, *Natl. Sci. Rev.* **2019**, *6*, 551.
[14] A. W. Li, M. C. Sobral, S. Badrinath, Y. Choi, A. Graveline, A. G. Stafford, J. C. Weaver, M. O. Dellacherie, T. Y. Shih, O. A. Ali, J. Kim, K. W. Wucherpfennig, D. J. Mooney, *Nat. Mater.* **2018**, *17*, 528.
[15] U. Sahin, Ö. Türeci, *Science* **2018**, *359*, 1355.
[16] J. Zhou, A. Y. Kroll, M. Holay, R. H. Fang, L. Zhang, *Adv. Mater.* **2020**, *32*, 1901255.
[17] H. Jiang, Q. Wang, X. Sun, *J. Controlled Release* **2017**, *267*, 47.
[18] D. J. Irvine, M. C. Hanson, K. Rakhra, T. Tokatlian, *Chem. Rev.* **2015**, *115*, 11109.
[19] H. Liu, K. D. Moynihan, Y. Zheng, G. L. Szeto, A. V. Li, B. Huang, D. S. Van Egeren, C. Park, D. J. Irvine, *Nature* **2014**, *507*, 519.
[20] B. Bodey, B. Bodey, Jr., S. E. Siegel, H. E. Kaise, *Anticancer Res.* **2000**, *20*, 2665.
[21] S. H. van der Burg, R. Arens, F. Ossendorp, T. van Hall, C. J. M. Melief, *Nat. Rev. Cancer* **2016**, *16*, 219.
[22] A. Ukidve, K. Cu, N. Kumbhojkar, J. Lahann, S. Mitragotri, *Drug Delivery Transl. Res.* **2021**, *342*, 2276.
[23] Q. Chen, L. Xu, C. Liang, C. Wang, R. Peng, Z. Liu, *Nat. Commun.* **2016**, *7*, 13193.
[24] L. Zhang, Y. Zhang, Y. Xue, Y. Wu, Q. Wang, L. Xue, Z. Su, C. Zhang, *Adv. Mater.* **2019**, *31*, 1805936.
[25] M. Chang, Z. Hou, M. Wang, C. Li, J. Lin, *Adv. Mater.* **2021**, *33*, 2004788.
[26] C. W. Ng, J. Li, K. Pu, *Adv. Funct. Mater.* **2018**, *28*, 1804688.

2108012 (11 of 12)

**ADVANCED
SCIENCE NEWS**

www.advancedsciencenews.com

**ADVANCED
MATERIALS**

www.advmat.de

[27] X. Li, J. F. Lovell, J. Yoon, X. Chen, *Nat. Rev. Clin. Oncol.* **2020**, *17*, 657.

[28] M. A. Shahbazi, T. D. Fernández, E. M. Mäkilä, X. L. Guével, C. Mayorga, M. H. Kaasalainen, J. J. Salonen, J. T. Hirvonen, H. A. Santos, *Biomaterials* **2014**, *35*, 9224.

[29] F. Fontana, M. A. Shahbazi, D. Liu, H. Zhang, E. M. Mäkilä, J. J. Salonen, J. T. Hirvonen, H. A. Santos, *Adv. Mater.* **2017**, *29*, 1603239.

[30] F. Fontana, M. Fusciello, C. Groeneveldt, C. Capasso, J. Chiaro, S. Feola, Z. Liu, E. M. Mäkilä, J. J. Salonen, J. T. Hirvonen, V. Cerullo, H. A. Santos, *ACS Nano* **2019**, *13*, 6477.

[31] F. Fontana, H. Lindstedt, A. Correia, J. Chiaro, O. K. Kari, J. Ndika, H. Alenius, J. Buck, S. Sieber, E. M. Mäkilä, J. J. Salonen, A. Urtti, V. Cerullo, J. T. Hirvonen, H. A. Santos, *Adv. Healthcare Mater.* **2020**, *9*, 2000529.

[32] B. Xia, W. Zhang, H. Tong, J. Li, Z. Chen, J. Shi, *ACS Biomater. Sci. Eng.* **2019**, *5*, 1857.

[33] Y. Su, X. Wei, F. Peng, Y. Zhong, Y. Lu, S. Su, T. Xu, S.-T. Lee, Y. He, *Nano Lett.* **2012**, *12*, 1845.

[34] G. Zhu, J.-T. Liu, Y. Wang, D. Zhang, Y. Guo, E. Tasciotti, Z. Hu, X. Liu, *ACS Appl. Mater. Interfaces* **2016**, *8*, 11881.

[35] H. Alhmoud, A. Cifuentes-Rius, B. Delalat, D. G. Lancaster, N. H. Voelcker, *ACS Appl. Mater. Interfaces* **2017**, *9*, 33707.

[36] A. H. Colby, R. Liu, R. P. Doyle, A. Merting, H. Zhang, N. Savage, N.-Q. Chu, B. A. Hollister, W. McCulloch, J. E. Burdette, C. J. Pearce, K. Liu, N. H. Oberlies, Y. L. Colson, M. W. Grinstaff, *J. Controlled Release* **2021**, *337*, 144.

[37] F. Belardelli, M. Ferrantini, *Trends Immunol.* **2002**, *23*, 201.

[38] T. D. Fernández, J. R. Pearson, M. P. Leal, M. J. Torres, M. Blanca, C. Mayorga, X. L. Guével, *Biomaterials* **2015**, *43*, 1.

[39] S. W. van Gool, J. Vermeiren, K. Rafiq, K. Lorré, M. de Boer, J. L. Ceuppens, *Eur. J. Immunol.* **1999**, *29*, 2367.

[40] L. J. Orchyl, J. D. Bazzill, C. Park, Y. Xu, R. Kuai, J. J. Moon, *Biomaterials* **2018**, *182*, 157.

[41] X. Han, S. Shen, Q. Fan, G. Chen, E. Archibong, G. Dotti, Z. Liu, Z. Gu, C. Wang, *Sci. Adv.* **2019**, *5*, eaaw6870.

[42] O. Veish, A. J. Vegas, *Adv. Drug Delivery Rev.* **2019**, *144*, 148.

[43] M. Tonigold, V. Mailänder, *Nanomedicine* **2016**, *11*, 2625.

[44] H. Shen, J. You, G. Zhang, A. Ziemys, Q. Li, L. Bai, X. Deng, D. R. Erm, X. Liu, C. Li, M. Ferrari, *Adv. Healthcare Mater.* **2012**, *1*, 84.

[45] F. Sallusto, J. Geginat, A. Lanzavechia, *Annu. Rev. Immunol.* **2004**, *22*, 745.

[46] E. J. Wherry, M. Kurachi, *Nat. Rev. Immunol.* **2015**, *15*, 486.

[47] N. Gong, N. C. Sheppard, M. M. Billingsley, C. H. June, M. J. Mitchell, *Nat. Nanotechnol.* **2021**, *16*, 25.

[48] E. Kolaczkowska, P. Kubes, *Nat. Rev. Immunol.* **2013**, *13*, 159.

[49] J. Li, L. Xie, B. Li, C. Yin, G. Wang, W. Sang, W. Li, H. Tian, Z. Zhang, X. Zhang, Q. Fan, Y. Dai, *Adv. Mater.* **2021**, *33*, 2008481.

[50] Y. Yue, F. Li, Y. Li, Y. Wang, X. Guo, Z. Cheng, N. Li, X. Ma, G. Nie, X. Zhao, *ACS Nano* **2021**, *15*, 15166.